Integrating Functional and Structural Brain Connectomes: a novel multilayer graphs framework for Alzheimer's disease classification

Carlo Ferritto[1], Giulia Lioi[2], Pierre-Yves Jonin[1,3], and Julie Coloigner[1],
for the Alzheimer's Disease Neuroimaging Initiative[*]
[1]Univ Rennes, CNRS, Inria, Inserm, IRISA UMR 6074, EMPENN — ERL U 1228, F-35000 Rennes, France
[2]IMT Atlantique, Lab-STICC UMR CNRS 6285, F-29238, Brest, France
[3]Neurology Department, Rennes University Hospital, Rennes, France

***Abstract*—Multilayer graphs are an emerging tool in connectomics and graph theory, offering a powerful framework to integrate and analyze multiple data modalities. By representing each modality as a separate layer with interconnecting edges, Multilayer graphs capture complex relationships that are often missed in classical unimodal graph analyses. This ability to combine complementary information is particularly valuable in clinical neuroscience, where both functional and structural connectivity provide distinct but related insights into pathophysiology. In this study, we present a novel Multilayer graphs framework to integrate functional MRI and diffusion MRI data for the classification of patients with Alzheimer's disease, mild cognitive impairment, and healthy controls using the Alzheimer's Disease Neuroimaging Initiative database. The novelty of our approach lies in assigning distinct weights to structural and functional layers, optimizing their respective contributions to classification. Results show that our Multilayer graphs framework improves classification accuracy while uncovering key brain regions and subnetworks. This work underscores the potential of multilayer graphs to provide a more comprehensive understanding of how Alzheimer's disease alters brain connectivity, and to enhance the detection of neurodegenerative disorders.**

***Index Terms*—Multilayer Graphs, Functional Connectivity, Structural Connectivity, Alzheimer's Disease**

I. Introduction

Alzheimer's disease (AD) is a neurodegenerative disorder characterized by a progressive cognitive decline, finally resulting in a loss of functional independence. Before the loss of independence, patients show impairments across several cognitive domains, most often including memory loss, a transitional stage coined "Mild Cognitive Impairment" (MCI) [1]. Neuroimaging studies using functional MRI (fMRI) and diffusion MRI (dMRI) have provided critical insights into the structural and functional brain alterations associated with AD [2], [3]. fMRI studies reveal disrupted functional connectivity, particularly in the default mode network (DMN), which is crucial for memory and self-referential processes [4]. dMRI, on the other hand, captures microstructural changes in white matter fibers, showing reduced fractional anisotropy and increased mean diffusivity in regions vulnerable to AD pathology, such as the medial temporal lobes (MTL) and the posterior cingulate cortex (PCC) [5], [6].

Graph theory has emerged as a powerful tool for modeling these interactions by representing the brain as a network where nodes correspond to brain regions and edges signify their connectivity [7]. Structural connectivity (SC) derived from dMRI reflects the physical white matter pathways linking brain regions, while functional connectivity (FC) obtained from resting-state fMRI (rs-fMRI) captures the statistical dependencies between neuronal activity across different brain areas [8]. Although these modalities provide complementary perspectives, most previous studies have relied on single-layer graphs representing SC or FC, which fail to capture the integrative nature of brain organization [9].

To better understand changes in connectivity related to AD, advanced analytical frameworks are needed to integrate both structural and functional alterations. Recent advances in Multilayer Graphs (MG) theory offer an innovative framework for modeling and analyzing complex, multimodal data [10]. MG extend traditional graph representations by integrating multiple interconnected layers, each representing a different data modality. This structure allows the preservation of within-modality relationships while simultaneously capturing inter-modality interactions. This approach is particularly relevant in the study of neurodegenerative diseases, where the interplay between structural damage and functional disruption could underlie disease progression, as suggested in [11].

Recent MG studies have shown that AD is associated with loss of centrality in the hippocampus and posterior DMN regions [12], as well as with loss of inter-frequency centrality in the PCC [13]. Despite the growing interest in MG, their application to classify neurodegenerative conditions remains unexplored. Existing literature predominantly focuses on unimodal analyses or simple combinations of features without explicitly modeling interdependencies [14], [15]. This gap highlights the need for advanced analytical frameworks

*Data used in preparation of this article were obtained from the Alzheimer's Disease Neuroimaging Initiative (ADNI) database (adni.loni.usc.edu). As such, the investigators within the ADNI contributed to the design and implementation of ADNI and/or provided data but did not participate in analysis or writing of this report. A complete listing of ADNI investigators can be found at: http://adni.loni.usc.edu/wp-content/uploads/how_to_apply/ADNI_Acknowledgement_List.pdf

Corresponding author: Julie Coloigner (julie.coloigner@irisa.fr)

capable of integrating SC and FC to improve classification accuracy, better discriminate between different stages of the disease (i.e. MCI or full-blown AD with loss of independence) and provide new insights into the underlying pathophysiology.

In this study, we present a novel MG framework that integrates rs-fMRI and dMRI data to classify AD, MCI, and healthy controls (HC). Our approach assigns different coefficients to SC and FC layers, optimizing their contribution to classification using a simplicial homology global optimisation (SHGO) algorithm [16]. These coefficients act as weighting factors, allowing the MG to balance the complementary information but distinct nature of SC and FC [9]. By optimizing these weights, we ensure that both modalities contribute effectively to classification, rather than being treated as equally important a priori. Furthermore, we leverage MG metrics such as overlapping strength and multiplex participation coefficient to capture the topological differences between groups [17].

II. Material

A. The dataset

Data used in the preparation of this article were obtained from the Alzheimer's Disease Neuroimaging Initiative (ADNI) database[1]. This cohort includes 42 HC, 34 MCI and 37 AD patients. The three groups were matched for sex (pairwise chi-squared test, $p > 0.5$), age (pairwise t-test, $p > 0.1$) and years of education (pairwise t-test, $p > 0.1$). Additionally, only amyloid-β positive MCI participants, as assessed through PET imaging [18], were included. Due to the well-acknowledged heterogeneity of MCI, this was aimed to increase the likelihood that AD is the underlying pathology responsible for cognitive decline [19]. For each participant, three brain MRI sequences were acquired: structural MRI, dMRI and rs-fMRI.

B. Preprocessing

The preprocessing of the images was carried out mainly using the open source medical image processing toolbox Anima[2] and the FMRIB Software Library (FSL) [20]. The structural MRI preprocessing pipeline contains skull-stripping and brain tissue segmentation of cerebrospinal fluid, white-matter and gray-matter using FSL's *fast*. The dMRI images were corrected for eddy currents, motion and distortion correction using the FSL's function *eddy*. The corresponding fieldmap was estimated either using two echo-planar images with opposing phase-encoding directions processed with FSL's *topup* or using fieldmap images if they were obtained during the acquisition phase. The images were then denoised using the NL-Means method [21] and skull stripped using the brain mask of the structural MRI. The dMRI images were then used to estimate the response function with the Dhollander method [22], followed by fiber orientation distribution (FOD) estimation with the MSMT-CSD approach [23] to model white matter, gray matter, and cerebrospinal fluid. Subsequently, tractography was performed using the iFOD2 algorithm [24] to generate 10 million streamlines, which were then filtered using the SIFT2 method [25] for tractogram refinement. The rs-fMRI images were motion and slice-time corrected using FSL's *mcflirt* and FSL's *slicetimer*. The images were corrected for distorsion using FSL's *fugue* and the same fieldmap as for dMRI images. Finally, the Schaefer atlas [26], which includes 400 cortical regions, and the Melbourne Subcortex atlas [27], which consists of 16 subcortical regions, were used for both dMRI and rs-fMRI to define regions of interest (ROIs). Based on these 416 ROIs, SC and FC were represented as matrices of size $N \times N$, where $N = 416$. While SC values represent the white-matter fiber density between regions, FC values correspond to the Pearson correlation between the average time series of each pair of ROIs.

[1] adni.loni.usc.edu

[2] https://github.com/Inria-Empenn/Anima-Public

III. Methods

A. Multilayer graphs

Let $\mathcal{M} = (\mathcal{G}, \mathcal{C})$ denote a multilayer graph where $\mathcal{G}$ is a set of graphs and $\mathcal{C}$ is a set of connections that link the vertices of different L graphs. Specifically, $\mathcal{G} = \{G_\alpha | \alpha \in \mathbb{N}\}$ where $G_\alpha = (V_\alpha, E_\alpha)$ is an undirected, weighted, and without self-loop graph at layer α. The relationship between the set of N vertices V_α and the set of $N(N-1)$ edges E_α can be characterized by an adjacency matrix $\mathbf{A} \in \mathbb{R}^{N \times N}$ with elements $A^\alpha_{i,j} = w^\alpha_{i,j}$ if an edge connects vertices i and j in layer α, and $A^\alpha_{i,j} = 0$ otherwise. The set of connections between the vertices of the graphs at different layers α and β is represented by $\mathcal{C} = \{E_{\alpha\beta} \subseteq V_\alpha \times V_\beta | \alpha \neq \beta\}$. The supra-adjacency matrix $\mathbf{S} \in \mathbb{R}^{NL \times NL}$ provides a practical and straightforward extension of the adjacency matrix to the multilayer graph case. Let $\mathcal{M}$ be a weighted and undirected multilayer graph with N vertices per layer and L layers, its supra-adjacency matrix $\mathbf{S}$ elements are $S^{\alpha\beta}_{ij} = w^{\alpha\beta}_{ij}$ if there is a connection between vertex i in layer α and vertex j in layer β, and $S^{\alpha\beta}_{ij} = 0$ otherwise. $\mathbf{S}$ can therefore be visualized as a block matrix where L blocks on the main diagonal account for within layer links, while $L(L-1)$ off-diagonal blocks account for interlayer links.

Specific instances of multilayer graphs are known as multiplexes. In a multiplex, interlayer links exist only between replica nodes. These connections indicate the corresponding nodes across different layers in the model. Thus, in a multiplex $V_\alpha = V, \alpha \in \{1, ..., L\}$ and $\mathcal{C} = \{E_{\alpha\beta} \subseteq \{(v, v) | v \in V\} | \alpha \neq \beta\}$. In this configuration, the off-diagonal blocks of $\mathbf{S}$ are filled by the $N \times N$ identity matrix.

B. Multiplex construction

In this study we built multiplexes using FC and SC matrices. This results in the following multiplex with $L = 2$ layers:

$$\mathcal{M} = \{A^{[\alpha]}, \forall \alpha \in \{\text{rs-fMRI, dMRI}\}\} \tag{1}$$

where $A^{[\alpha]}$ is the adjacency matrix for the modality α. To reduce the influence of spurious fibers, all connections with less than 2 fibers were eliminated from SC matrices. Similarly, all negative connections in the FC matrices were also deleted, as suggested in [28]. In addition, the SC matrices edges

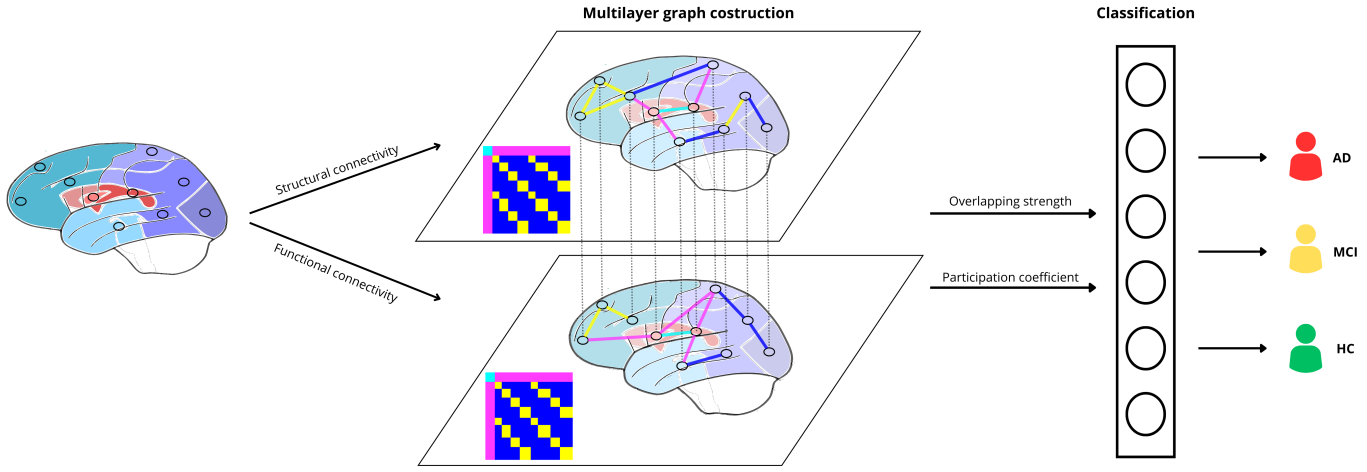

Fig. 1. Framework pipeline. Cortical (blue) and subcortical (red) regions are segmented into 416 ROIs. The structural layer is derived from dMRI (density of white matter fibers), while the functional layer is constructed using the Pearson correlation coefficient between rs-fMRI time series. Each layer is assigned four coefficients to adjust the edge weights both within and between the cortical and subcortical networks and the latter are optimized through the SHGO algorithm. The two layers are linked through replica nodes, and the resulting MG are used to compute the strength and multiplex participation coefficient, which are then utilized for the classification task.

were log-transformed to account for the skewed distribution. Both connectivity matrices were then thresholded using a consistency-based method to retain only the top 25% most consistent edges [29]. Since the weights in each layer may span different ranges, we applied a min-max normalization to each layer. This normalization scales all edge weights to the interval $[0, 1]$, allowing for direct comparison across layers. To effectively capture differential connectivity patterns in the MG, we assigned four distinct weighting coefficients to each layer. These coefficients regulate the relative influence of specific network components, ensuring that both FC and SC contribute meaningfully to the classification task (see III-D). Specifically, we distinguished between (i) connectivity within cortical networks, (ii) connectivity between different cortical networks, (iii) connectivity within the subcortical network, and (iv) connectivity between cortical and subcortical regions. These connections correspond to the yellow, blue, light blue, and fuchsia links in Fig. 1, respectively. Intra-cortical connections facilitate local processing, while inter-cortical connections enable large-scale integration across brain regions. In contrast, subcortical structures play crucial roles in memory, motor control, and emotional regulation. Connectivity within these subcortical regions and with cortical regions offers insights into the integrity of essential circuits, which are notably affected in AD [6]. However, determining the optimal balance between these connectivity types is non-trivial, as their relative contributions to classification may vary across different disease stages. To address this, we employed the SHGO algorithm [16]. Each potential solution in the SHGO algorithm represents a set of weighting coefficients x defined as coordinates of the 8-dimensional search space, where each dimension is bounded between 0 and 1. To guide this optimization process, we formulated a fitness function F based on Fisher's criterion, which measures the separability between groups:

$$F(x) = \frac{(\overline{M}_{G_1}(x) - \overline{M}_{G_2}(x))^2}{s^2_{G_1} - s^2_{G_2}} \tag{2}$$

where $\overline{M}_{G_1}(x)$ and $\overline{M}_{G_2}(x)$ represent the mean of a metric for the two groups and $s^2_{G_1} = \sum_{s \in G_1}(M_s(x) - \overline{M}_{G_1}(x))^2$. This fitness function ensures that the optimization process prioritizes solutions that maximize the difference between groups while minimizing within-group variability.

C. Metrics

Several metrics have been proposed in the literature to measure MG properties [10], [17] in terms of centrality, modularity, segregation or integration and efficiency. To quantify the difference between the groups, we leveraged two relevant multiplex metrics: the overlapping strength and the multiplex participation coefficient, which have previously been used to identify the loss of inter-frequency hubs in fMRI [13] and MEG [12] studies employing MG. The single α layer strength measures the importance of a node in a specific layer and is defined as $k_i^\alpha = \sum_{i \neq j} A_{ij}^\alpha$, while the overlapping strength measures the importance of a node across-layer and is defined as $os_i = \sum_\alpha \sum_{i \neq j} S_{ij}^{\alpha\alpha}$. According to this definition, the higher the overlapping strength value, the more important a node is in the multiplex network. On the other hand, the multiplex participation coefficient measures the connectivity similarity pattern across layers and is defined as $mpc_i = \frac{L}{L-1}[1 - \sum_{\alpha=1}^{L}(\frac{k_i^\alpha}{o_i})^2]$, where L is the number of layers in the multiplex. In this formulation mpc_i ranges from 0 to 1 and indicates how uniformly the links of node i are distributed across layers. Specifically, $mpc_i = 0$ if all edges of node i are confined to a single layer, while $mpc_i = 1$ if the edges are evenly distributed across all L layers, with higher values indicating a greater balance of node i connections among the layers.

D. Classification

Once we have found the optimal configuration of coefficients for each feature, we can compute and use them for the classification task. We trained three different binary classifiers to perform pairwise classification of the considered groups: HC vs. MCI, HC vs. AD and MCI vs. AD. We then evaluated the performance of 4 different classifiers: k-nearest neighbors (KNN), support vector machine (SVM), Logistic Regression (Logit) and Multi-layer Perceptron (MLP). The classifiers were trained using a Leave-One-Out Cross-Validation (LOOCV) scheme and their performance were evaluated using the test set balanced accuracies. Incremental feature selection was carried out adding one feature to the subset of features at each step according to the ANOVA ranking. The classification performance of our Weighted Multiplexes (WMP) using overlapping strength (*os*) and multiplex participation coefficient (*mpc*) were compared to other three methods: Un-Weighted Multiplexes (UWMP) using the same features as WMP, Single-Layer Structural Graph (SSG) and Single-Layer Functional Graph (SFG) using strength (*k*).

IV. Results and Discussion

TABLE I
COMPARISON OF TEST BALANCED ACCURACIES.

Method	HC vs. MCI	HC vs. AD	MCI vs. AD	Average
WMP$_{os}$	61.3%	82.2%	69.1%	70.8%
WMP$_{mpc}$	67.5%	83.4%	75.1%	**75.3**%
WMP$_{os+mpc}$	**69.8**%	**83.6**%	72.0%	75.1%
UWMP$_{os}$	63.7%	77.3%	71.8%	70.9%
UWMP$_{mpc}$	63.7%	78.5%	71.8%	71.3%
UWMP$_{os+mpc}$	67.2%	79.5%	71.8%	72.8%
SFG$_k$	62.0%	71.9%	69.1%	67.7%
SSG$_k$	59.8%	**83.7**%	**77.4**%	73.6%
SFG$_k$ + **SSG**$_k$	60.7%	81.0%	**77.4**%	73.0%

Since all classifiers performed similarly, Table I reports the highest test set balanced accuracy achieved in the classification tasks using the LOOCV scheme. Overall, our method outperforms the other approaches on average. In more details, our WMP framework achieved the highest accuracy for HC vs. MCI classification task, suggesting that multimodal integration and weighting may be more sensitive to subtle connectivity changes related to the earliest stages of the disease. Our method performs at the level of single-layer graphs for the HC vs. AD comparison, but achieves slightly lower accuracies than SSG or combined SSG and SFG for the MCI vs. AD classification task. Fig. 2 illustrates the contribution of different coefficients to the optimization problem for the HC vs. AD classification task. When using the participation coefficient, the SC coefficient between subcortical and cortical regions emerges as the most important, along with the FC coefficient within cortical regions, suggesting their crucial role in distinguishing AD from HC. However, when using the overlapping strength as metric, the highest weight is assigned to FC within sub-cortical regions, indicating that alterations in subcortical network integration are particularly relevant for AD classification. Fig. 3 highlights the contribution of different brain regions for the HC vs. AD classification task. Recent research highlights the crucial role of subcortical regions in AD, showing that their structural and functional alterations

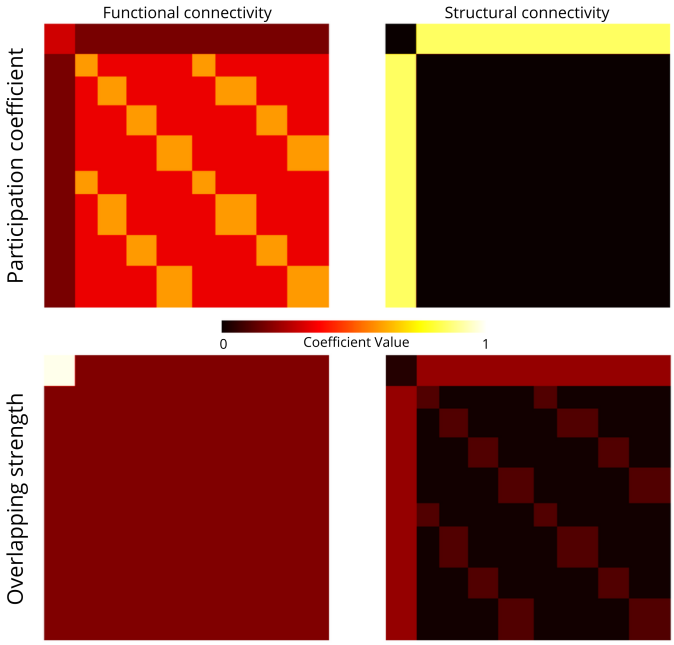

Fig. 2. Mean value of coefficients for the HC vs AD classification task using Participation coefficient (top figure) and Overlapping strength (bottom figure).

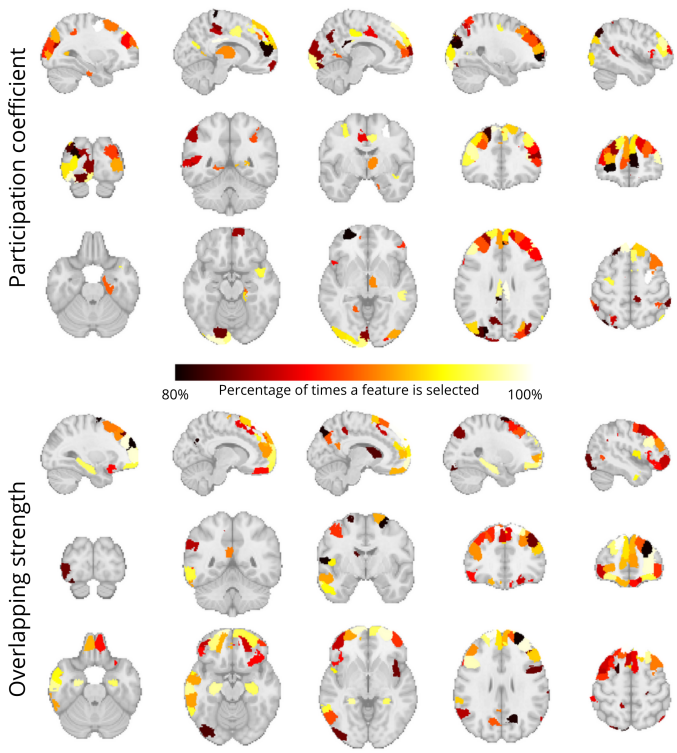

Fig. 3. Most selected features using Participation coefficient (top figure) and Overlapping Strength (bottom figure) for HC vs AD classification task. The results highlight the top 20% of features that were selected most often during the LOOCV scheme, indicating their relative importance.

play a key part in disease progression [30]. AD is characterized by pathophysiological changes which lead to neuronal loss in the MTL, including the hippocampus[3], whose degeneration results in memory loss. In line with findings in the literature for both dMRI [15], fMRI [14] and MG [31] studies, our results show that the hippocampus and the regions from the DMN, are the most critical regions for the classification between HC and AD using overlapping strength. When classification relies on the multiplex participation coefficient, the selected regions sometimes differ, likely because this metric captures connectivity similarity patterns across modalities, emphasizing the integration of different layers while de-emphasizing local, single-layer properties.

V. Conclusion

This study presents a novel MG framework for integrating rs-fMRI and dMRI data to classify between AD, MCI, and HC patients. By optimizing the contributions of SC and FC layers through a SHGO algorithm, the proposed framework achieves promising improvement in the identification of AD, especially in its earliest clinical stages, compared to unimodal approaches. The results highlight the importance of cortical-subcortical connectivity, particularly involving the hippocampus and DMN regions, in distinguishing between disease stages. Results demonstrate the potential of MG to enhance our understanding of brain connectivity alterations in neurodegenerative diseases and improve early detection of AD. For future work, we aim to expand our framework by incorporating additional MG metrics to better capture various brain properties and apply them to the classification of other neurodegenerative diseases, such as Parkinson's disease.

References

[1] P. Scheltens, et al., "Alzheimer's disease," *The Lancet*, vol. 397, no. 10284, pp. 1577–1590, 2021.

[2] G. B. Frisoni, N. C. Fox, C. R. Jack, P. Scheltens, and P. M. Thompson, "The clinical use of structural MRI in Alzheimer disease," *Nature Reviews Neurology*, vol. 6, no. 2, pp. 67–77, 2010.

[3] R. Sperling, "The potential of functional MRI as a biomarker in early Alzheimer's disease," *Neurobiology of aging*, vol. 32, no. Suppl 1, pp. S37–S43, 2011.

[4] M. D. Greicius, G. Srivastava, A. L. Reiss, and V. Menon, "Default-mode network activity distinguishes Alzheimer's disease from healthy aging: Evidence from functional MRI," *Proceedings of the National Academy of Sciences*, vol. 101, no. 13, pp. 4637–4642, 2004.

[5] D. Salat, et al., "White Matter Pathology Isolates the Hippocampal Formation in Alzheimer's Disease," *Neurobiology of aging*, vol. 31, no. 2, pp. 244–256, 2010.

[6] Y. Zhou, J. H. Dougherty, K. F. Hubner, B. Bai, R. L. Cannon, and R. K. Hutson, "Abnormal connectivity in the posterior cingulate and hippocampus in early Alzheimer's disease and mild cognitive impairment," *Alzheimer's & Dementia*, vol. 4, no. 4, pp. 265–270, 2008.

[7] E. Bullmore and O. Sporns, "Complex brain networks: graph theoretical analysis of structural and functional systems," *Nature Reviews Neuroscience*, vol. 10, no. 3, pp. 186–198, 2009.

[8] O. Sporns, "Structure and function of complex brain networks," *Dialogues in Clinical Neuroscience*, vol. 15, no. 3, pp. 247–262, 2013.

[9] J. S. Damoiseaux and M. D. Greicius, "Greater than the sum of its parts: a review of studies combining structural connectivity and resting-state functional connectivity," *Brain Structure and Function*, vol. 213, no. 6, pp. 525–533, 2009.

[3]The hippocampus is a cortical structure, but we classified it as 'subcortical' following common brain atlas terminology.

[10] M. De Domenico, et al., "Mathematical Formulation of Multilayer Networks," *Physical Review X*, vol. 3, no. 4, pp. 041022, 2013.

[11] J. Guillon, et al., "Disrupted core-periphery structure of multimodal brain networks in Alzheimer's disease," *Network Neuroscience*, vol. 3, no. 2, pp. 635–652, 2019.

[12] M. Yu, et al., "Selective impairment of hippocampus and posterior hub areas in Alzheimer's disease: an MEG-based multiplex network study," *Brain*, vol. 140, no. 5, pp. 1466–1485, 2017.

[13] J. Guillon, et al., "Loss of brain inter-frequency hubs in Alzheimer's disease," *Sci Rep*, vol. 7, no. 1, pp. 10879, 2017.

[14] B. Ibrahim, et al., "Diagnostic power of resting-state fMRI for detection of network connectivity in Alzheimer's disease and mild cognitive impairment: A systematic review," *Human Brain Mapping*, vol. 42, no. 9, pp. 2941–2968, 2021.

[15] L. Billeci, A. Badolato, L. Bachi, and A. Tonacci, "Machine Learning for the Classification of Alzheimer's Disease and Its Prodromal Stage Using Brain Diffusion Tensor Imaging Data: A Systematic Review," *Processes*, vol. 8, no. 9, pp. 1071, 2020.

[16] S. C. Endres, C. Sandrock, and W. W. Focke, "A simplicial homology algorithm for Lipschitz optimisation," *Journal of Global Optimization*, vol. 72, no. 2, pp. 181–217, 2018.

[17] F. Battiston, V. Nicosia, and V. Latora, "Structural measures for multiplex networks," *Physical Review E*, vol. 89, no. 3, pp. 032804, 2014.

[18] W. J. Jagust, et al., "The Alzheimer's Disease Neuroimaging Initiative 2 PET Core: 2015," *Alzheimer's & Dementia*, vol. 11, no. 7, pp. 757–771, 2015.

[19] M. S. Albert, et al., "The diagnosis of mild cognitive impairment due to Alzheimer's disease: Recommendations from the National Institute on Aging-Alzheimer's Association workgroups on diagnostic guidelines for Alzheimer's disease," *Alzheimer's & Dementia*, vol. 7, no. 3, pp. 270–279, 2011.

[20] M. Jenkinson, C. F. Beckmann, T. E. J. Behrens, M. W. Woolrich, and S. M. Smith, "FSL," *NeuroImage*, vol. 62, no. 2, pp. 782–790, 2012.

[21] N. Wiest-Daesslé, S. Prima, P. Coupé, S. P. Morrissey, and C. Barillot, "Rician noise removal by non-Local Means filtering for low signal-to-noise ratio MRI: applications to DT-MRI," *Internation Conference on Medical image computing and computer-assisted intervention : MICCAI*, vol. 11, no. Pt 2, pp. 171–179, 2008.

[22] T. Dhollander, D. Raffelt, and A. Connelly, "Unsupervised 3-tissue response function estimation from single-shell or multi-shell diffusion MR data without a co-registered T1 image," in *ISMRM workshop on breaking the barriers of diffusion MRI*. 2016, vol. 5, Lisbon, Issue: 5.

[23] B. Jeurissen, J.-D. Tournier, T. Dhollander, A. Connelly, and J. Sijbers, "Multi-tissue constrained spherical deconvolution for improved analysis of multi-shell diffusion MRI data," *NeuroImage*, vol. 103, pp. 411–426, 2014.

[24] J. D. Tournier, F. Calamante, and A. Connelly, "Improved probabilistic streamlines tractography by 2nd order integration over fibre orientation distributions," in *Proceedings of the international society for magnetic resonance in medicine*. 2010, vol. 1670, Stockholm.

[25] R. E. Smith, J. D. Tournier, F. Calamante, and A. Connelly, "SIFT2: Enabling dense quantitative assessment of brain white matter connectivity using streamlines tractography," *NeuroImage*, vol. 119, pp. 338–351, 2015.

[26] A. Schaefer, et al., "Local-Global Parcellation of the Human Cerebral Cortex from Intrinsic Functional Connectivity MRI," *Cerebral Cortex*, vol. 28, no. 9, pp. 3095–3114, 2018.

[27] Y. Tian, D. Margulies, M. Breakspear, and A. Zalesky, "Topographic organization of the human subcortex unveiled with functional connectivity gradients," *Nature Neuroscience*, vol. 23, no. 11, pp. 1421–1432, 2020.

[28] M. Rubinov and O. Sporns, "Complex network measures of brain connectivity: Uses and interpretations," *NeuroImage*, vol. 52, no. 3, pp. 1059–1069, 2010.

[29] J. A. Roberts, A. Perry, G. Roberts, P. B. Mitchell, and M. Breakspear, "Consistency-based thresholding of the human connectome," *NeuroImage*, vol. 145, pp. 118–129, 2017.

[30] A. Shukla, R. Tiwari, and S. Tiwari, "Analyzing subcortical structures in Alzheimer's disease using ensemble learning," *Biomedical Signal Processing and Control*, vol. 87, pp. 105407, 2024.

[31] A. Canal-Garcia, et al., "Multiplex connectome changes across the alzheimer's disease spectrum using gray matter and amyloid data," *Cerebral Cortex*, vol. 32, no. 16, pp. 3501, 2022.